

SIMULATING THE LYMAN ALPHA FOREST

Marie E. Machacek

Department of Physics, Northeastern University, Boston, MA 02115

Greg L. Bryan

Princeton University Observatory, Princeton, NJ 08544

Peter Anninos

*Laboratory for Computational Astrophysics, National Center for
Supercomputing Applications, 405 Matthews Ave, Urbana, IL 61801*

Avery Meiksin

*Institute of Astronomy, University of Edinburgh
Royal Observatory, Blackford Hill, Edinburgh EH9 3HJ, UK*

Michael L. Norman

*Astronomy Department, University of Illinois at Urbana-Champaign
Urbana, IL 61801*

In this paper we review the importance of the Lyman alpha forest as a probe of structure formation in the universe. We first discuss the statistics used to describe the Lyman alpha forest and the numerical techniques used to produce simulated spectra of the forest from a given cosmological model. We then discuss the physical picture of the absorbing structures that emerges from these numerical simulations. Finally, we comment on how two of the statistics, the slope of the column density distribution and the b parameter distribution, may be used to constrain competing cosmologies.

1 Introduction

Technological advances over the past two decades have resulted in a wealth of new, good quality observations that allow us for the first time to quantitatively as well as qualitatively constrain cosmological models. Among this data are high resolution spectra of quasar light¹ that reveal hundreds of absorption features blueward of the Lyman alpha emission peak ($\lambda = 121.56701$ nm in the rest frame of the quasar's neutral hydrogen, but appropriately redshifted due to cosmological expansion). Usually a handful of the narrowest features can be identified with heavy elements such as iron or carbon. Occasionally the spectrum contains a broad saturated feature, most probably associated with a galactic halo, where the integrated number density of neutral hydrogen along the observer's line of sight (the HI column density) may exceed 10^{21} cm⁻². However, the vast majority of the spectral lines are due to the absorption of

quasar light by intervening neutral hydrogen of much lower column densities, 10^{12} to 10^{17} cm^{-2} . For redshifts $z \geq 3$ this “Lyman alpha forest” accounts for more than 90% of all the baryons allowed by nucleosynthesis. Thus these lines map the distribution and properties of matter in the universe at a time when structure is rapidly forming yet before most of the baryons have collapsed into highly nonlinear objects such as galaxies and galaxy clusters. This gives the Lyman alpha forest a unique place in the study of structure formation. The data enjoy other advantages as well. Since the quasar distribution does not pick out a preferred direction in the sky, the quasar lines of sight randomly sample the universe. The data also provide good statistics since the spectrum from each quasar line of sight typically contains hundreds of Lyman alpha forest lines.

2 Statistics of the Forest

The quantity measured directly by observers is the flux F , defined as the transmission probability of light as a function of wavelength, or equivalently velocity, along a given line of sight. Once the continuum has been determined, absorption lines in the resulting spectrum are usually fit using Voigt profile functions. For HI the gaussian component dominates and may be characterised by the HI column density (N_{HI}) and the Doppler width parameter b for the line. In order to connect the spectrum to the underlying properties of the absorbing medium, it is useful to consider the optical depth τ related to F by $F = \exp(-\tau)$ where τ depends on the HI density distribution along the line of sight, particle velocities and the Lyman alpha absorption cross section.² These quantities can be computed from numerical simulations, as discussed below, and thus be used to compare model predictions with observation.

Statistical measures are needed to characterize the properties of the hundreds of observed lines in a given spectrum. These statistics fall into two main classes, those that depend upon the line fitting procedure and those that work directly with the raw distribution of flux. Historically most observational data were analysed in terms of the statistics of the Voigt profile line fit. We will focus on two of the most common statistics of this kind, N_{HI} and the b parameter distributions. The N_{HI} distribution is defined to be the number of lines per unit wavelength per column density interval of neutral hydrogen. The amplitude of the distribution is not useful to discriminate between models because it scales, up to a weak temperature dependence, as $(\Omega_b h^2)^2 / \Gamma$ where h is the dimensionless Hubble parameter in units of 100 km/s/Mpc, Ω_b is the fraction of the critical density carried in baryons, and Γ is the photoionization rate at the Lyman alpha edge. Since Γ is not well known, this scale factor is usually taken

as a free parameter determined from the data by either fitting the amplitude of the N_{HI} distribution at a particular point or computing the average flux decrement at a given redshift. The slope of the N_{HI} distribution is, however, a robust statistic that can be used to test models. The data are well fit by a power law with slope $\beta = -1.5$ for column densities below 10^{14} cm^{-2} , but the distribution steepens for higher column densities. A second statistic, the b parameter distribution, counts the number of lines per unit redshift of a given Doppler width. These distributions are more challenging to interpret. This is due, in part, to the fact that the fit itself is not unique. Many of the absorption features found in the data are blends of two or more lines. Furthermore the connection between the b distribution and the properties of the medium is complex. Absorber temperature, gas velocity (Hubble flow and physical) and density profile all contribute to the line width. Because of these difficulties new statistics based directly on the raw flux distribution have been proposed.³ These include the flux probability distribution and moments of the n -point flux distribution. Although these statistics have the advantage that they are independent of any line fitting program, their major disadvantage is that little data have yet to be analysed in this way. We discuss these line independent statistics in more detail elsewhere.^{4,5} In either case numerical simulations of synthetic spectra and their subsequent analysis provide the link between the observed spectrum and the underlying cosmological model.

3 Simulation Strategy

We consider a suite of the currently most promising hierarchical cosmological models characterized by the dimensionless Hubble parameter h , the fraction Ω of the critical density carried in each model component (baryonic gas, cold and/or hot dark matter, cosmological constant), and the slope n of the initial power spectrum of density fluctuations. The models⁵ include the standard cold dark matter model (SCDM), a flat cold dark matter model with nonvanishing cosmological constant (LCDM), a low density cold dark matter model (OCDM), a flat cold dark matter model with a tilted power spectrum (TCDM), and a critical model with both cold and hot (two massive neutrinos) dark matter components (CHDM). The SCDM, OCDM, and LCDM model parameters agree with earlier simulations by Zhang, *et al.*⁶ TCDM and CHDM model parameters are taken from the Grand Challenge Cosmology Consortium model comparison project. The initial fluctuation spectra, assumed to be gaussian, are normalized using the observed distribution of galaxies, although all but SCDM are also consistent with measurements of the cosmic microwave background.

We use a single grid Eulerian code (KRONOS) with a particle-mesh gravity solver and a modified piecewise parabolic method to simulate the gas hydrodynamics to evolve the system nonlinearly to moderate redshifts $z \simeq 2$.⁷ The radiation field, assumed spatially constant, is computed from the observed quasar distribution⁸ with spectral index $\alpha = 1.5$ which reionizes the universe around $z \sim 6$ and peaks at $z \simeq 2$. Since nonequilibrium effects can be important, we calculate radiative processes such as photoionization, recombination and Compton cooling for six chemical species (HI, HII, HeI, HeII, HeIII, e) using the method of Anninos, *et al.*⁹ However, we do not include radiative transfer, self-shielding, star formation, or feedback from star formation and so can not address the physics within the highest density clumps ($N_{HI} \geq 10^{16} \text{ cm}^{-2}$). We use 256^3 grid cells in a simulation box of length 9.6 Mpc comoving with the universal expansion and follow the evolution of 128^3 (256^3) dark matter (gas) particles, respectively. This results in a spatial resolution of 37.5 kpc and mass resolutions of $2.9 \times 10^7 M_\odot$ ($3.6 \times 10^6 M_\odot$) for the dark matter (gas) particles.

The output from numerical simulations of cosmological models are three-dimensional snapshots of the state of the universe as the universe ages (redshift z decreases). For each z chosen the simulation returns the positions and velocities for each particle, the temperature, pressure, and gas density, and the distribution of each chemical species throughout the box. By taking slices through the simulation box we can directly compare the physical properties of matter in the box. In particular the distribution of neutral hydrogen traces well the baryon gas distribution even though by $z \simeq 5$ the universe is almost completely reionized with the fraction of gas remaining neutral $\leq 10^{-4}$. Furthermore the gas distribution traces well the cold dark matter distribution so that probing neutral hydrogen by use of Lyman alpha absorption is indeed mapping the matter distribution in the universe. In order to generate synthetic quasar absorption spectra from the simulation data, we place a quasar within the box that is well removed from the box edges. We then trace the absorption of Lyman alpha radiation from the quasar by the neutral hydrogen in the box along 300 randomly generated lines of sight. The spectra, i.e. transmitted flux as a function of velocity or wavelength, so produced can be analysed in the same way as the observational data, and the statistics, after averaging over the 300 lines of sight, compared with observation.

There is a tension in simulations of the Lyman alpha forest between the need for large simulation box size to include sufficient large scale power from the density fluctuations and the need for high spatial resolution to adequately model the absorbing structures. We use SCDM as a typical hierarchical model to systematically study these numerical uncertainties.⁴ By varying the simulation box length by factors of two from 2.4 Mpc to 19.2 Mpc at 75 kpc fixed

spatial resolution, we find that the physical properties and statistical measures of the gas discussed above are nearly identical for the largest two box sizes demonstrating convergence by 9.6 Mpc. The major difference due to the presence of larger scale modes in the bigger boxes is an increase in the amount of high temperature gas due to shock heating around the edges of the more dense sheets, filaments and knots. This has little effect on the low density regions responsible for the forest. Similarly we study the effects of spatial resolution by fixing the box size at 2.4 Mpc (small so that we could obtain high grid resolution) and decreasing the grid spacing by factors of two from 75 kpc to 18.75 kpc. The physical properties of the gas are again quite similar. However there is a slight tendency for the higher resolutions to have more low density gas due to more small scale power and a better ability to resolve small scale features. Since lower density regions are cooler due to expansion cooling and reduced photo-ionization, higher grid resolution also systematically produces more low-temperature gas. Again these differences have little effect on the column density distributions for neutral hydrogen showing the robust nature of this statistic. On the other hand, the b parameter distribution systematically decreases with increased resolution, although its shape remains largely invariant. Similar resolution dependence appears in fit independent statistics such as the first moment of the 2-point flux distribution. Thus this effect is not an artifact of the line fitting procedure. We argue instead that the principle cause of this resolution dependence is numerical thickening of the density profile for low spatial resolution. The b parameter and fit independent statistics do appear to be converging at our highest spatial resolutions. However, it is clear that a spatial resolution of 37.5 kpc is just barely sufficient to model these distributions.

4 Physical Picture

A consistent picture of the Lyman alpha forest in cold dark matter dominated cosmologies is now emerging from numerical simulations^{6,10} using a variety of numerical techniques and from more analytical approximations.^{11,2} In this picture the absorbers that produce lines with low column densities $N_{HI} < 10^{15} \text{ cm}^{-2}$ at $z \approx 3$ are large, unvirialized objects of size ~ 100 kpc and low densities comparable to the cosmic mean¹² that have grown by gravitational amplification from primordial density fluctuations. In order to refine this picture we select those cells from the SCDM simulations⁴ that correspond to a line in a given column density range and compute the mean characteristic (dark matter δ_{dm} and gas δ_b overdensities, temperature, and peculiar velocity) profiles across these structures. These are plotted for $z = 3$ in Figure 1. From

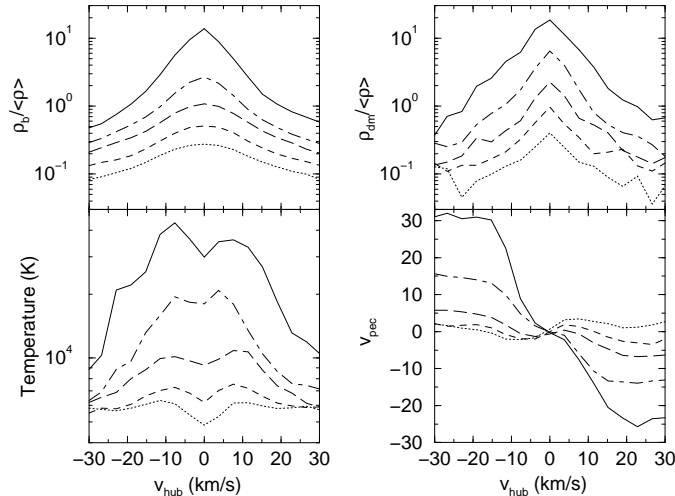


Figure 1: Mean profiles at $z = 3$ for baryon overdensity, dark matter overdensity, gas temperature and peculiar velocity distributions projected along the line of sight for (bottom to top) $\log(N_{\text{HI}}) = 12, 12.5, 13, 13.5, 14.5$.

the overdensity profiles we see that these structures range from underdense structures ($\delta \sim 0.2$) for $N_{\text{HI}} = 10^{12}$ to mildly nonlinear structures ($\delta \approx 10$) for $N_{\text{HI}} = 10^{14.5}$. In all cases the wings of the profile drop below the cosmic mean. This means that most low column density lines are produced by absorbers located in voids. The velocity plot indicates that these absorbers are infalling in comoving coordinates. However, the infall velocities for absorbers with $N_{\text{HI}} \leq 10^{13.5}$ in this model are less than the Hubble expansion so that these lowest column density structures are actually expanding in absolute coordinates. Once the column density exceeds 10^{14} cm^{-2} , the qualitative character of the absorber changes. The infall velocity becomes greater than the Hubble flow so that the object has collapsed.

A careful study of the central regions of these profiles also reveals interesting physics. The dark matter and gas density profiles are remarkably similar, except near the peak where the gas exhibits a rounded rather than cuspy shape. When the gas was heated at reionization to roughly 15,000 K, gas in the center of the peaks found itself overpressured and started to expand. This expansion is seen as a kink with positive slope at the center of the velocity profiles for the lower column densities and causes the smoothing of the peak of the gas density distribution relative to that for dark matter. The central gas cooled

as it expanded causing a corresponding dip at the center of the temperature profile. As the column density increases, pressure is less effective against gravity in causing the central gas to expand. Thus the kink in the velocity profile flattens, the dip in the temperature profile is diminished and the peak in the density profile becomes more pronounced. At the highest column densities, $N_{HI} \sim 10^{14} \text{ cm}^{-2}$, when the absorber changes from an uncollapsed to a collapsed system, two shocks form on either side of the absorber midplane and propagate outwards. This can be seen in the velocity distribution at $\pm 10 \text{ km/s}$ and in the twin shock-heated peaks in the temperature distribution. It is intriguing to note that this qualitative change in the character of the absorber occurs near the column density where carbon abundances are observed to increase dramatically¹³ and where the column density distribution appears to steepen.

5 Testing Cosmological Models

In order to use the Lyman alpha forest to discriminate between competing cosmologies we need to use our physical understanding of the nature of the absorbers to link the measured statistics to the characteristic properties that define the model. The column density distribution is an integrated quantity relatively insensitive to the detailed shape of the HI density profile or spatial resolution of the simulation. The slope of the column density distribution is primarily determined by the power carried in fluctuations on small $\sim 200 - 500 \text{ kpc}$ scales with less power producing steeper slopes. One measure of this small scale power, σ_{34} , is the *rms* density fluctuation computed from the linearly evolved power spectrum at the redshift of interest filtered by a scale roughly half of the Jean's length.¹⁴ In Figure 2 we plot the slope of the N_{HI} distribution versus σ_{34} for $z = 3$. As this figure shows, agreement with observations is found for several popular models and favors those models with more power at smaller scales.

The b parameter distribution at $z = 3$ is shown in Figure 3. The shape of this distribution is well reproduced by hierarchical cosmologies and follows closely the analytic profile, $b^{-5} \exp(-b_\sigma^4/b^4)$, of Hui & Rutledge¹⁵ based on the gaussian nature of the underlying density and velocity fields. However, for our choices of SCDM, LCDM, and OCDM models, the predicted medians b_σ are substantially too low.⁵ In order to search for a remedy, we need to understand which of the competing physical processes sets the scale of the b parameter for low column density absorbers. Returning to Figure 1 we see that the gas temperatures are too low for thermal Doppler broadening to dominate any but the narrowest of lines. Similarly the velocities for the gas

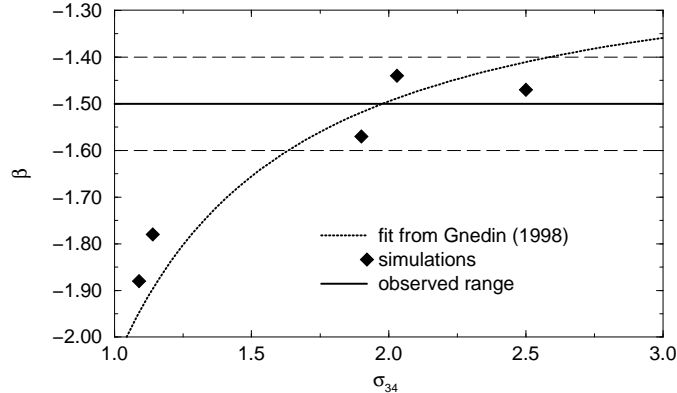


Figure 2: Slope of the column density distribution at $z = 3$ as a function of σ_{34} . Simulation models are from left to right: TCDM, CHDM, SCDM, LCDM, OCDM

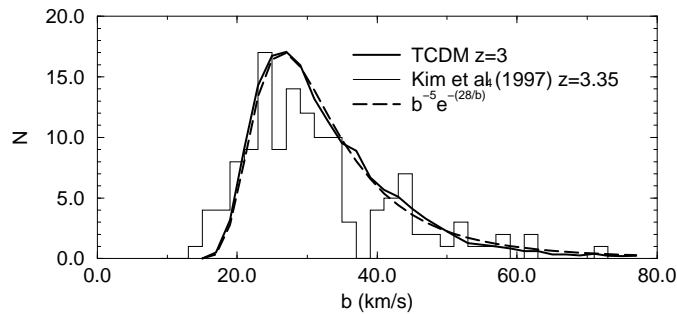


Figure 3: b parameter distributions for observational data at mean $z = 3.35$, TCDM simulation at redshift $z = 3$, and the analytical profile (dashed) $b^{-5} \exp(-b_{\sigma}^4/b^4)$ with $b_{\sigma} = 28$.

are small and an increase in the physical infall velocity would serve to narrow, rather than broaden, the line. Thus the dominating contributor to the width of the forest lines is the shape of the density distribution itself. This shape could be changed by increased thermal pressure within the gas, but such a large temperature increase seems difficult to obtain.⁴ Instead we may search for key changes in the density distribution affecting the b distribution due to the differing power spectra of competing cosmologies. Thus the Lyman alpha forest holds tremendous promise as a sensitive probe of structure formation as our understanding of the connections between the spectra and the underlying absorbers continues to improve.

Acknowledgments

This work is done under the auspices of the Grand Challenge Cosmology Consortium and supported in part by NSF grant ASC-9318185 and NASA Astrophysics Theory Program grant NAG5-3923.

References

- [1] D. Kirkman and D. Tytler, *Astrophysical Journal* **484**, 672 (1997); E. Hu, T. Kim, L.L. Cowie, A. Songaila, *Astronomical Journal* **110**, 1526 (1995); L. Lu, W.L.W. Sargent, D.S. Womble, M. Takada-Hidai, *Astrophysical Journal* **471**, 582 (1996); T. Kim, E.M. Hu, L.L. Cowie, A. Songaila, *Astronomical Journal* **114**, 1 (1997).
- [2] L. Hui, N.Y. Gnedin, Y. Zhang *Astrophysical Journal* **486**, 599 (1997).
- [3] J. Miralda-Escude, *et al*, to appear in Proceedings of 13th IAP Colloquium: Structure and Evolution of the IGM from QSO Absorption Line Systems, eds. P. Petitjean, S. Charlot, 1997; R. Cen, *Astrophysical Journal* **479**, L85 (1997).
- [4] G.L. Bryan, M.E. Machacek, P. Anninos, M.L. Norman, preprint astro-ph/9805340, submitted to *Astrophysical Journal*, 1998.
- [5] M.E. Machacek *et al*, in preparation, 1998.
- [6] Y. Zhang, P. Anninos, M.L. Norman, *Astrophysical Journal* **453**, L57 (1995); Y. Zhang, "Cosmological hydrodynamics simulations of the Lyman Alpha forest", PhD. Thesis, University of Illinois, 1996.
- [7] G.L. Bryan, M.L. Norman, J.M. Stone, R. Cen, J.P. Ostriker, *Comput. Phys. Comm.* **89**, 149 (1995).
- [8] F. Haardt, P. Madau, *Astrophysical Journal* **461**, 20 (1996).
- [9] P. Anninos, Y. Zhang, T. Abel, M.L. Norman, *New Astronomy* **2**, 209 (1997).
- [10] R. Cen, J. Miralda-Escude, J.P. Ostriker, M. Rauch, *Astrophysical Journal* **437**, L9 (1994); L. Hernquist, N. Katz, D.H. Weinberg, J. Miralda-Escude, *Astrophysical Journal* **457**, 51L (1996).
- [11] H.G. Bi, *Astrophysical Journal* **405**, 479 (1993); H.G. Bi, A. Davidsen, *Astrophysical Journal* **479**, 523 (1997); N.Y. Gnedin, L. Hui, *MNRAS* **296**, 44 (1998).
- [12] Y. Zhang, A. Meiksin, P. Anninos, M.L. Norman, *Astrophysical Journal* **495**, 63 (1998).
- [13] L.Lu, W.L.W. Sargent, T.A. Barlow, M. Rauch, preprint astro-ph/9802189, 1998.
- [14] N.Y. Gnedin, preprint astro-ph/9706286, submitted to *MNRAS*, 1998.
- [15] L. Hui, R.E. Rutledge, preprint astro-ph/9709100, 1998.